Available online at www.sciencedirect.com
SCIENCE DIRECT®
Journal of Sound and Vibration 283 (2005) 749–763
JOURNAL OF SOUND AND VIBRATION
www.elsevier.com/locate/jsvi

Flexural vibration of rectangular plates subjected to sinusoidally distributed compressive loading on two opposite sides

K.K.V. Devarakonda, C.W. Bert*

School of Aerospace and Mechanical Engineering, The University of Oklahoma, 865 Asp ave., Felgar Hal, Room 212, Norman, OK 73019-1052, USA

Received 1 October 2003; accepted 11 May 2004
Available online 15 December 2004

Abstract

Natural frequencies and mode shapes of rectangular plates subjected to sinusoidally distributed in-plane compressive loading on two opposite edges were considered in this work. Although vibration analysis of rectangular plates was investigated by numerous authors, flexural vibration of plates with nonlinearly distributed in-plane loading received much less attention. However, certain problems involving thermal stresses may have such nonlinear loading conditions in the plane of the plate. The analysis procedure for the title problem involves first finding a plane elasticity solution for the in-plane problem satisfying all boundary conditions. Then using this in- plane solution, flexural vibration analysis has to be carried out. In a related work investigated recently by the present authors, an in-plane elasticity solution was developed and was compared with existing analytical solutions in the literature and with the finite element method. One aspect of this study was the stress diffusion (i.e., reduction of stress) phenomenon along the length of the plate as well as the presence of all three in-plane stress components. Using this in-plane solution, vibration analysis of rectangular plates was carried out for various plate aspect ratios and the results were compared with corresponding values from finite element analysis.

*Corresponding author. Tel.: +1 405 325 5011; fax: +1 405 325 1088.
E-mail address: cbert@ou.edu (C.W. Bert).

0022-460X/$ - see front matter © 2004 Elsevier Ltd. All rights reserved.
doi:10.1016/j.jsv.2004.05.029

1. Introduction

Vibration analysis of thin rectangular plates subjected to uniform and linearly varying in-plane load has been studied extensively in the literature [1,2]. Although exact solutions existed for plates where the in-plane load was uniform, until recently only approximate solutions existed for plate vibration problems involving linearly varying in-plane loads including moment loads. Recently, Leissa and Kang [3,4] obtained exact series solutions for buckling and natural frequencies of rectangular plates subjected to *linearly* varying in-plane load. The case of nonlinearly varying in-plane load in the x direction received less attention partly due to additional complexity of solving the plane elasticity problem satisfying the necessary boundary conditions. Timoshenko and Goodier [5] were the first ones to propose an approximate in-plane solution for the case of a parabolically varying in-plane load, using trial functions which satisfied all the boundary conditions exactly. Pickett [6] considered the same problem and obtained a solution satisfying the equilibrium and compatibility equations, but some residual stresses remained at the boundaries. Apparently unaware of the in-plane stress solutions as developed by Timoshenko and Goodier and by Pickett, van der Neut [7] and Benoy [8] used an over-simplified in-plane solution for the buckling analysis wherein they considered the x direction in-plane stress distribution to be the same at every x coordinate position and the y direction normal stress and the shear stress τ_{xy} to be zero.

Based on the mechanics of the problem, in accordance with Saint-Venant's principle, one can expect that the in-plane stresses inside the plate should exhibit the stress diffusion phenomenon as the plate aspect ratio is increased. It is to be noted that the plane elasticity solutions as obtained by Timoshenko and Goodier and by Pickett showed stress diffusion at higher plate aspect ratios along with the presence of σ_y and τ_{xy} stresses throughout the plate.

More recently the present investigators [9,10] obtained an in-plane solution in connection with the buckling problem of a plate having sinusoidal in-plane load, and the results were compared with the existing analytical solutions in the literature as well as with the finite element solution. Two different analytical solutions were obtained using the superposition method and it was observed that the renormalized two-stress-function solution showed better boundary condition satisfaction compared to the four-stress-function solution. In the present analysis, both the in-plane analytical solutions developed previously are used for the plate vibration problem and the results are compared with the finite element solution.

2. In-plane solution

As shown in Fig. 1, a rectangular plate of dimensions (a and b) in the x and y directions, respectively, is considered. The coordinate system is placed at the center of the plate and the compressive in-plane loading applied at the edges $\xi = \pm 1$ is

$$\sigma_x = \sigma_0 \cos\left(\frac{\pi\eta}{2}\right). \tag{1}$$

Here $\eta = 2y/b$ and $\xi = 2x/a$, with range $[-1 \leqslant (\xi, \eta) \leqslant +1]$, are the dimensionless coordinates of the plate.

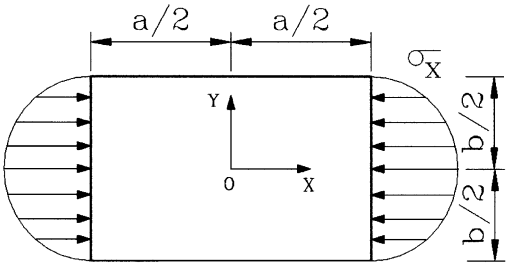

Fig. 1. Geometry and loading of the plate.

Recently, the present authors [9,10] described in detail a renormalized two-stress-function solution and a four-stress-function solution based on the superposition method and the results were compared with a finite element solution. The superposition method, as suggested by Timoshenko and Goodier [5] and extensively used by Gorman and Singhal [11], involves superposing two or more stress function solutions in such a way that the residual stresses (usually at the boundaries) are cancelled. Each stress function solution is considered in terms of a trigonometric function in either plate coordinate. By expanding the stress functions in terms of Fourier series at the plate boundaries, one can superpose the stresses in such a way that the plate boundary conditions are satisfied. It is to be noted that due to the Fourier expansion of the stress functions, the superposition method is a series solution.

In the present case considering the Airy stress function ϕ_1 as

$$\phi_1 = f(\xi)\cos\left(\frac{\pi\eta}{2}\right) \tag{2}$$

and substituting into the governing differential equation $\nabla^4\varphi = 0$, one can obtain the general solution for the functional $f(\xi)$ as

$$f(\xi) = C_1\cosh\left(\frac{k\pi\xi}{2}\right) + C_2\sinh\left(\frac{k\pi\xi}{2}\right) + C_3\xi\cosh\left(\frac{k\pi\xi}{2}\right) + C_4\xi\sinh\left(\frac{k\pi\xi}{2}\right), \tag{3}$$

where $k = a/b$ (plate aspect ratio) and C_1–C_4 are constants which are to be obtained from the boundary conditions. It is to be noted that the stress function solution as given by Eqs. (2) and (3) gives a zero normal stress at $\eta = \pm 1$ edges.

Substituting the zero-shear-stress boundary condition and the normal stress distribution as defined in Eq. (2), (after eliminating C_2 and C_3 based on symmetry conditions) at the edges $\xi = \pm 1$, yields a complete solution for the stress function φ_1:

$$f(\xi) = C_1\cosh\left(\frac{k\pi\xi}{2}\right) + C_4\xi\sinh\left(\frac{k\pi\xi}{2}\right), \tag{4}$$

where

$$C_1 = \frac{\pi a/2b\cosh(\pi a/2b) + \sinh(\pi a/2b)}{\pi a/2b + \sinh(\pi a/2b)\cosh(\pi a/2b)}\frac{\sigma_o b^2 h}{\pi^2}, \tag{5}$$

$$C_4 = -\frac{\pi a/2b \sinh(\pi a/2b)}{\pi a/2b + \sinh(\pi a/2b)\cosh(\pi a/2b)} \frac{\sigma_o b^2 h}{\pi^2}. \tag{6}$$

However, the above in-plane stress solution gives a residual shear stress distribution at the $\eta = \pm 1$ edges which can be expanded as a Fourier sine series. In order to eliminate these shear stresses, one can start with a second stress function solution, which produces sinusoidal shear stress distribution in the x direction. After eliminating the unsymmetric components, this stress function is given by

$$\phi_2 = \sum_{m=1,2\ldots} \left(D_{1m} \cosh\left(\frac{m\pi\eta}{k}\right) + D_{4m}\eta \sinh\left(\frac{m\pi\eta}{k}\right)\right) \cos(m\pi\xi), \tag{7}$$

where D_{1m} and D_{4m} are constants to be determined from boundary conditions and the residual stress from the previous stress function solution φ_1. The complete results for the constants D_{1m} and D_{4m} and the stress distribution are given in Appendix A.

It is to be observed that whereas the initial stress-function solution (φ_1) is a one-term solution, the second stress-function solution (φ_2) is a series solution. Although the stress-function solution φ_2 has zero normal stresses at the $\eta = \pm 1$ edges and zero shear stresses at $\xi = \pm 1$ edges, it does produce a residual normal stress (σ_x) at $\xi = \pm 1$ edges.

It is observed that the residual normal stress due to the above stress function solution φ_2 is merely shifting the edge stress distribution by a constant value. In view of this, a renormalization factor is introduced by combining a uniform stress and a multiplication factor in such a way that the σ_x boundary conditions are satisfied on $\xi = \pm 1$ edges.

Thus the complete solution is

$$\varphi = (\varphi_1 + \varphi_2 + R)r, \tag{8}$$

where R is the uniform stress and r the renormalization factor such that the edge stress distribution satisfies Eq. (1).

The four-stress-function solution can be considered as an extension of the two-stress-function method wherein the residual stresses are removed by superposing additional stress function

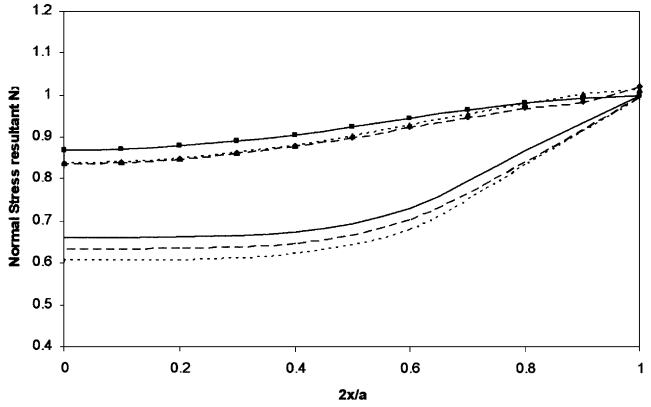

Fig. 2. Comparative in-plane σ_x stress distribution (at $2y/b = 0$) along plate half length for different plate aspect ratios: —, two-stress-function; - - -, four-stress-function; ....., FEA; lines with markers are for $k = 1$; without markers $k = 3$.

solutions instead of renormalization. It was observed from the previous analysis [10] that the four-stress-function showed some residual stresses especially at the plate corners. However, the distribution of stresses throughout the plate is in close agreement with the two-stress-function approach and with the finite element analysis (Fig. 2). In the present analysis, both two- and four-stress-function solutions are considered for the vibration analysis and the results are compared with the finite element analysis.

3. Vibration analysis

The governing differential equation for vibration of thin isotropic plates subjected to compressive in-plane loading is

$$\nabla^4 w + \frac{h}{D}\left(\sigma_x \frac{\partial^2 w}{\partial x^2} + 2\tau_{xy}\frac{\partial^2 w}{\partial x \partial y} + \sigma_y \frac{\partial^2 w}{\partial y^2} + \rho \frac{\partial^2 w}{\partial t^2}\right) = 0, \tag{9}$$

where D is the flexural rigidity, h is the plate thickness, and w is the normal deflection, and ρ is the plate density. After considering

$$w(x, y, t) = \overline{w}(x, y) \sin \omega t$$

one can write the above equation as

$$\nabla^4 \overline{w} + \frac{h}{D}\left(\sigma_x \frac{\partial^2 \overline{w}}{\partial x^2} + 2\tau_{xy}\frac{\partial^2 \overline{w}}{\partial x \partial y} + \sigma_y \frac{\partial^2 \overline{w}}{\partial y^2} - \rho\omega^2 \overline{w}\right) = 0. \tag{10}$$

As the in-plane stress solution is a series solution, an exact analytical solution may not be possible due to the complexity of the resulting plate vibration equation. Therefore, an approximate solution using the Galerkin method is obtained for combinations of simply supported and clamped rectangular plate edges. For simply supported rectangular plates with central coordinate system the trial functions in Eq. (11a) below satisfy all the required boundary conditions. However, in order to obtain consecutive modes, trial functions involving sinusoidal terms have also to be considered as shown in Eq. (11b). The trial functions for clamped plates are given in Eqs. (12a) and (12b).

$$\phi_{SS} = \cos\frac{m\pi\xi}{2} \quad \text{for } m = 1, 3, 5, \ldots \text{ modes}, \tag{11a}$$

$$\phi_{SS} = \sin\frac{n\pi\xi}{2} \quad \text{for } n = 2, 4, 6, \ldots \text{ modes}, \tag{11b}$$

$$\phi_C = \left(\cos\frac{m\pi\xi}{2} + \cos\frac{(m+2)\pi\xi}{2}\right) \quad \text{and } m = 0, 2, 4, \ldots \quad \text{for } 1, 3, 5, \ldots \text{ modes}, \tag{12a}$$

$$\phi_C = -\left(\sin\frac{n\pi\xi}{2} + \sin\frac{(n+2)\pi\xi}{2}\right) \quad \text{and } n = 1, 3, 5, \ldots \quad \text{for } 2, 4, 6, \ldots \text{ modes}. \tag{12b}$$

Similar functions in the y (or η) coordinate direction are obtained by replacing the x (or ξ) coordinate with y (or η) coordinate.

Also the Galerkin trial function corresponding to any mode (m, n) is

$$\phi_{mn} = a_{mn}\phi_m(\xi)\phi_n(\eta). \tag{13}$$

Free-vibration frequencies are obtained at various relative load (buckling load fraction) increments. Four trial functions involving (1,1), (2,1) (3,1), (4,1) vibration modes are considered in the present analysis.

4. Finite element analysis

The rectangular plate is modeled using an eight-node (MARC^{TM} element number 72) quadrilateral shell element. Although this element formulation is a generalized one for shell analysis, plate analysis can be done with equal ease. This element has three degrees of freedom at each corner node and an additional rotational degree of freedom at each mid-node on the four edges.

The plate model is analyzed using two different mesh sizes. A coarse mesh consisting of 200 (20×10 for plate aspect ratio of 3) elements and fine mesh consisting of 800 (40×20 in case of plate aspect ratio of 3) are considered. Care is taken to ensure that the element shape remains as close to the square as possible. The X and Y (u, v correspondingly) displacements are restricted along the nodes on two mutually perpendicular lines intersecting the plate surface. At the left and right edges of the plate, a uniform initial edge load (per unit length) is applied. This uniform edge load is different for each element such that the magnitude of the edge load follows a sinusoidal distribution. The edge load for each element is calculated such that the total edge load of the element is identically equal to that of total sinusoidal load corresponding to the element edge coordinates. Natural frequencies of vibration are calculated at various load increments and the results are tabulated.

5. Numerical results

Numerical computations are carried out using the first four consecutive modes in the x direction while keeping the first mode in the y direction and the results are compared with the finite element analysis. Figs. 3–6 show the dimensionless frequency ratio (Ω^2/Ω_s^2) against dimensionless in-plane load $(\sigma_0 h b^2/D)$ for various combinations of simply supported and clamped plate edges. The dimensionless quantity Ω is associated with the lowest natural frequency for the plate in consideration and Ω_s is the dimensionless fundamental frequency of an unloaded square plate with the corresponding edge condition. The frequency is nondimensionalized,

$$\Omega^2 = \frac{\rho h \omega^2 a^2 b^2}{D}. \tag{14}$$

In all the edge conditions, the plate frequencies of vibration using two- and four-stress-function methods showed close agreement with the finite element results only at lower plate aspect ratios. As the aspect ratio is increased, considerable differences were observed.

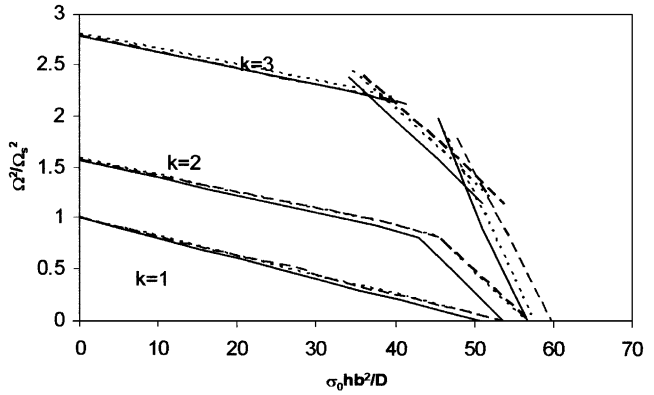

Fig. 3. Dimensionless frequency ratio at various in-plane load ratios for all edges simply supported (SSSS); $k = a/b$ (aspect ratio); —, two-stress-function; - - -, four-stress-function; ....., FEA.

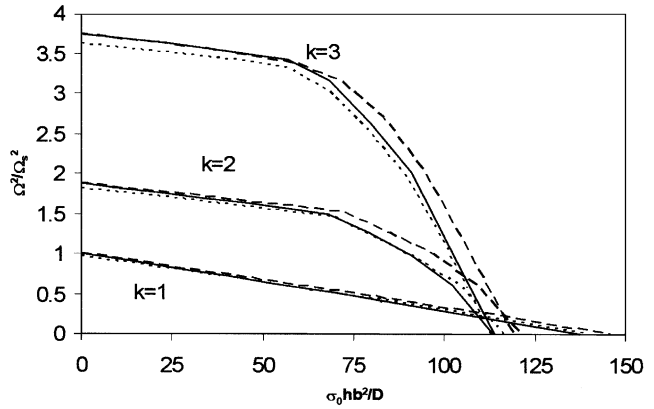

Fig. 4. Dimensionless frequency ratio at various in-plane load ratios for all edges clamped (CCCC); $k = a/b$ (aspect ratio); —, two-stress-function; - - -, four-stress-function; ....., FEA.

At higher aspect ratios, the two-stress-function method results appeared to be closer to the finite element results for SSSS and CCCC plates. It is interesting to note that the finite element frequencies are lower than the analytical results in the case of CCCC, SSCC plates and vice versa for the case of SSSS and CCSS plates.

Only in the case of SSCC plates having an aspect ratio of 3, the two-stress-function solution results and the four-stress-function results showed close agreement compared with the finite element frequencies throughout the in-plane load range. In general, the differences in frequency ratios between various methods increased uniformly as the in-plane load was increased towards the fundamental buckling load. Also these differences are more pronounced at higher plate aspect ratios. Thus one can see from these figures (Figs. 3–6) that larger differences in numerical values among the various methods of solution occurred for higher loads and higher plate aspect ratios.

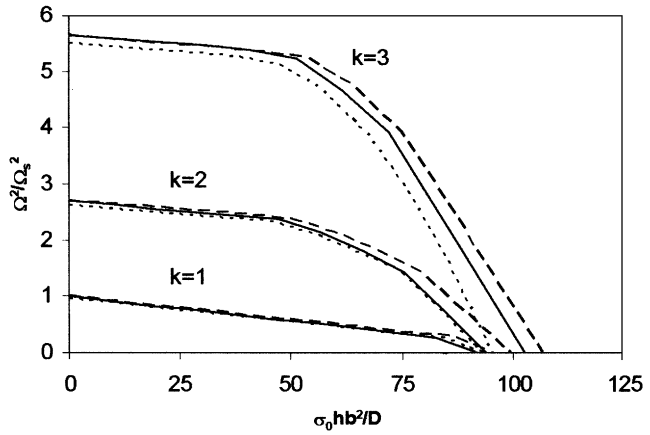

Fig. 5. Dimensionless frequency ratio at various in-plane load ratios for loaded edges simply supported and other edges clamped (SSCC); $k = a/b$ (aspect ratio); —, two-stress-function; - - -, four-stress-function; ....., FEA.

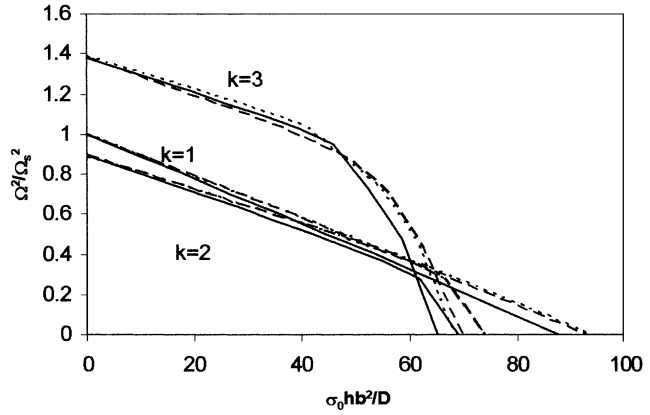

Fig. 6. Dimensionless frequency ratio at various in-plane load ratios for loaded edges clamped and other edges simply supported (CCSS); $k = a/b$ (aspect ratio); —, two-stress-function; - - -, four-stress-function; ....., FEA.

It is interesting to note that use of nondimensional frequency, as defined in Eq. (14), resulted in a lower value of fundamental frequency for the plate aspect ratio of 2 than that of a square plate for CCSS boundary conditions. All the remaining edge conditions gave higher frequencies than the fundamental frequency of the corresponding square plate.

Obviously, one can anticipate much closer agreement of the numerical values if one considers the nondimensional frequency itself, rather than the square of the frequency. Tables1(a)–4(c) show the numerical values of the nondimensional frequency at various in-plane load ratios. From these tables the excellent agreement between the two- and four-stress-function results is easily evident. Although there are minor differences in buckling loads [10] between these analytical methods, the vibration frequencies are identical when compared against the relative load ratio.

Table 1
Dimensionless frequency $\Omega = \omega ab\sqrt{\rho h/D}$, all edges simply supported (SSSS)

σ_0/σ_{cr}	Two-stress-function	Four-stress-function	Finite element analysis [a]
(a) $a/b = 1$			
0.1	18.72	18.72	18.80(1,1)
	47.64	47.63	48.05(2,1)
	96.78	96.77	98.59(3,1)
	165.7	165.7	171.3(4,1)
0.5	13.96	13.96	14.03 (1,1)
	40.12	40.05	40.43(2,1)
	88.74	88.66	90.41(3,1)
	157.5	157.5	162.9(4,1)
0.9	6.248	6.250	6.312(1,1)
	30.82	30.65	30.97(2,1)
	79.89	79.73	81.39(3,1)
	148.9	148.7	154.1(4,1)
$\sigma_{cr}hb^2/D$	50.78	53.49	53.75
(b) $a/b = 2$			
0.1	23.95	23.96	24.06(1,1)
	37.47	37.47	37.64(2,1)
	61.30	61.30	61.67(3,1)
	95.40	95.40	96.25(4,1)
0.5	20.81	20.89	20.97(1,1)
	28.00	28.04	28.16(2,1)
	48.30	48.29	48.56(3,1)
	80.94	80.90	81.68(4,1)
0.9	12.59	12.63	12.76(2,1)
	16.90	17.00	17.04(1,1)
	30.23	30.24	30.17(3,1)
	63.30	63.23	63.84(4,1)
$\sigma_{cr}hb^2/D$	53.64	56.77	56.55
(c) $a/b = 3$			
0.1	32.36	32.33	32.53(1,1)
	40.98	40.99	41.20(2,1)
	56.17	56.17	56.51(3,1)
	78.31	78.29	78.96(4,1)
0.5	30.12	29.96	30.31(1,1)
	32.83	32.89	33.20(2,1)
	41.88	41.87	42.35(3,1)
	60.05	59.94	60.91(4,1)
0.9	18.70	18.72	19.36(3,1)
	21.17	21.12	21.73(2,1)
	27.75	27.40	27.99(1,1)
	33.32	33.09	34.53(4,1)
$\sigma_{cr}hb^2/D$	56.73	59.69	57.54

[a]Modes are not consecutive.

Table 2
Dimensionless frequency $\Omega = \omega ab\sqrt{\rho h/D}$, loaded edges simply supported and other edges clamped

σ_0/σ_{cr}	Two-stress-function	Four-stress function	Finite element analysis
(a) $a/b = 1$			
0.1	28.40	28.42	27.86(1,1)
	52.97	52.97	52.25(2,1)
	100.2	100.2	100.5(3,1)
	168.3	168.3	172.1(4,1)
0.5	22.96	23.07	22.42(1,1)
	39.49	39.50	38.99(2,1)
	84.93	84.92	85.69(3,1)
	152.7	152.6	157.1(4,1)
0.9	15.65	15.90	15.12(1,1)
	17.67	17.68	17.58(2,1)
	66.26	66.24	67.67(3,1)
	135.2	135.2	140.1(4,1)
$\sigma_{cr}hb^2/D$	92.10	95.56	93.50
(b) $a/b = 2$			
0.1	48.03	48.06	47.31(1,1)
	56.89	56.91	55.86(2,1)
	75.83	75.84	74.54(3,1)
	106.4	106.3	105.1(4.1)
0.5	45.62	45.74	44.98(1,1)
	46.32	46.40	45.76(2,1)
	56.64	56.69	56.17(3,1)
	82.13	82.12	82.09(4,1)
0.9	25.18	25.15	25.56(3,1)
	30.24	29.67	30.58(2,1)
	43.45	43.79	42.99(1,1)
	48.40	48.52	50.06(4,1)
$\sigma_{cr}hb^2/D$	94.20	99.19	92.96
(c) $a/b = 3$			
0.1	69.93	69.87	68.93(1,1)
	75.02	75.06	73.82(2,1)
	85.19	85.25	83.75(3,1)
	102.2	102.1	100.6(4,1)
0.5	67.61	67.92	66.96(2,1)
	68.31	68.07	67.40(1,1)
	68.75	69.06	68.53(3,1)
	76.40	76.30	76.93(4,1)
0.9	33.966	34.00	36.71(4,1)
	46.877	47.85	39.60(3,1)
	56.91	60.30	59.83(2,1)
	66.662	66.09	66.04(1,1)
$\sigma_{cr}hb^2/D$	102.8	106.5	95.31

Table 3
Dimensionless frequency $\Omega = \omega ab\sqrt{\rho h/D}$, all edges clamped (CCCC)

σ_0/σ_{cr}	Two-stress-function	Four-stress-function	Finite element analysis
(a) $a/b = 1$			
0.1	34.97	34.97	34.38(1,1)
	71.27	71.21	70.44(2,1)
	132.19	132.1	130.0(3,1)
	212.74	212.6	213.2(4,1)
0.5	26.54	26.54	26.24(1,1)
	54.04	53.66	54.08(2,1)
	112.12	111.66	111.5(3,1)
	191.64	191.1	193.8(4,1)
0.9	12.31	12.32	12.35(1,1)
	27.17	25.80	29.11(2,1)
	87.76	86.70	89.30(3,1)
	167.9	166.9	172.4(4,1)
$\sigma_{cr}hb^2/D$	137.3	145.5	139.8
(b) $a/b = 2$			
0.1	49.45	49.48	48.63(1,1)
	62.51	62.52	61.11(2,1)
	88.92	88.63	85.39(3,1)
	126.0	126.0	121.9(4,1)
0.5	46.00	46.17	45.28(1,1)
	49.44	49.55	48.50(2,1)
	66.39	66.36	64.37(3,1)
	99.05	98.84	96.15(4,1)
0.9	28.90	28.97	28.37(3,1)
	30.25	30.76	29.37(2,1)
	43.72	43.90	43.03(1,1)
	61.54	60.87	60.56(4,1)
$\sigma_{cr}hb^2/D$	113.4	121.0	116.0
(c) $a/b = 3$			
0.1	70.50	70.42	69.42(1,1)
	77.45	77.50	75.88(2,1)
	91.60	91.72	88.58(3,1)
	113.0	113.0	109.0(4,1)
0.5	67.91	67.44	66.88(1,1)
	68.30	68.49	67.10(2,1)
	72.52	73.33	71.00(3,1)
	84.72	84.87	82.41(4,1)
0.9	37.20	37.09	36.68(4,1)
	44.44	46.31	40.90(3,1)
	59.37	60.19	57.81(2,1)
	66.39	65.83	66.30(1,1)
$\sigma_{cr}hb^2/D$	113.7	118.7	112.6

Table 4
Dimensionless frequency $\Omega = \omega ab\sqrt{\rho h/D}$, loaded edges clamped and other edges simply supported (CCSS)

σ_0/σ_{cr}	Two-stress-function	Four-stress-function	Finite element analysis
(a) $a/b = 1$			
0.1	27.65	27.65	27.61(1,1)
	67.48	67.46	67.59(2,1)
	129.7	129.69	128.9(3,1)
	210.8	210.8(4,1)	[a]—
0.5	20.76	20.75	20.83(1,1)
	56.77	56.65	56.97(2,1)
	117.5	117.4	117.1(3,1)
	198.0	197.9(4,1)	[a]—
0.9	9.382	9.379	9.537(1,1)
	43.41	43.12	43.62(2,1)
	104.0	103.7	104.4(3,1)
	184.4	184.1	186.9(4,1)
$\sigma_{cr}hb^2/D$	87.70	92.84	93.36
(b) $a/b = 2$			
0.1	26.52	26.54	26.52(1,1)
	45.30	45.30	45.10(2,1)
	76.22	76.21	74.58(3,1)
	116.6	116.6	114.5(4,1)
0.5	22.03	22.11	22.18(1,1)
	33.90	33.88	33.91(2,1)
	61.00	60.91	59.78(3,1)
	99.77	99.59	97.99(4,1)
0.9	15.27	15.25	15.44(2,1)
	15.57	15.82	15.70(1,1)
	40.70	40.45	39.89(3,1)
	79.45	79.02	77.94(4,1)
$\sigma_{cr}hb^2/D$	68.92	73.81	73.72
(c) $a/b = 3$			
0.1	33.50	33.39	33.54(1,1)
	45.02	45.02	44.86(2,1)
	64.98	65.02	63.61(3,1)
	91.47	91.36	89.69(4,1)
0.5	30.40	29.73	30.53(1,1)
	35.19	35.10	35.26(2,1)
	48.75	49.01	48.12(3,1)
	71.64	71.01	70.41(4,1)
0.9	20.01	19.07	19.88(2,1)
	20.52	19.98	20.53(3,1)
	28.89	28.80	29.09(1,1)
	44.12	42.56	43.60(4,1)
$\sigma_{cr}hb^2/D$	65.28	69.55	68.05

[a]Modes are not consecutive.

Table 5
Dimensionless frequency $\Omega = \omega ab\sqrt{\rho h/D}$ of a plate with an aspect ratio of 3 and relative in-plane load ratio of 0.5

Mode sequence	SSSS	SSCC	CCCC	CCSS
1	30.31(1,1)	66.96(2,1)	66.88(1,1)	30.53(1,1)
2	33.20(2,1)	67.40(1,1)	67.10(2,1)	35.26(2,1)
3	42.35(3,1)	68.53(3,1)	71.00(3,1)	48.12(3,1)
4	60.91(4,1)	76.93(4,1)	82.41(4,1)	70.41(4,1)
5	88.38(5,1)	95.45(5,1)	104.7(5,1)	101.5(5,1)
6	122.7(1,2)	124.7(6,1)	137.8(6,1)	123.0(1,2)
7	124.1(6,1)	163.9(7,1)	181.0(7,1)	132.2(2,2)
8	130.8(2,2)	189.5(1,2)	189.7(1,2)	140.8(6,1)
9	144.2(3,2)	195.2(2,2)	196.0(2,2)	147.5(3,2)
10	163.9(4,2)	204.1(3,2)	206.1(3,2)	169.6(4,2)

It is to be noted that in all the tables, the numerical values for nondimensional frequency are given based on the definition of Eq. (14). Also, the mode number shown in brackets for finite element results is applicable to the entire row (i.e. for both of the analytical methods). The only exception is the case of the CCSS plate (Table 4(a)) with an aspect ratio of 1.

As the Galerkin method is an assumed mode approximate method, one generally does not know beforehand whether or not the assumed modes yield consecutive modes. However, the finite element analysis arranges the modes consecutively based on the ascending order of the numerical value of the frequency. For comparison purposes, only those modes that are used for the analytical method are shown in all of these tables. The only exception is the lowest frequency for any given relative load ratio where all of the methods considered in the present study gave identical modes. Thus, with the exception of the lowest frequency, one can anticipate additional vibration modes to be active between the tabulated values. As a result of these additional modes, the frequency corresponding to the vibration mode (4,1) in Table 4(a) is not shown for the finite element results.

Table 5 lists the vibration frequencies in ascending order for various plate edge conditions (aspect ratio 3) subjected to a relative in-plane load of 0.5. It is to be noted that these values are listed based on the finite element analysis.

It is interesting to note the similarities in numerical frequencies for the first few modes between those plates which have common Y-type edge conditions. At higher modes, the frequencies are progressively higher for plates with clamped edge conditions than the corresponding values for simply supported edges.

6. Conclusions

Vibration analysis of a rectangular plate subjected to uniaxial nonlinear (sinusoidal) in-plane loading is carried out in the present work. Based on the in-plane elasticity solution developed previously [9,10], the vibration analysis is carried out and the results are compared with the finite element analysis. Due to the complexity of the governing differential equation, an approximate

solution using the Galerkin method is carried out. The variation of the lowest (fundamental) frequency with the buckling load is plotted for various combinations of simply supported and clamped rectangular plates, specifically SSSS, CCCC, SSCC, CCSS plates.

In general, excellent agreement for the frequencies between the analytical and the finite element results is observed. The differences among various methods are more pronounced at higher plate aspect ratios and with increasing in-plane loads.

Appendix A. Two-stress-function results

Let

$$\theta = \frac{\pi}{2ab}\left(\left(C_1\frac{k\pi}{2}+C_4\right)\sinh\frac{k\pi\xi}{2}+C_4\frac{k\pi}{2}\xi\cosh\frac{k\pi\xi}{2}\right) \tag{A.1}$$

and

$$F_{1m} = \int_{-1}^{1}\theta\,\sin(m\pi\xi)\,\mathrm{d}\xi, \quad m = 1,2,\ldots, \tag{A.2}$$

$$D_{1m} = \frac{-F_{1m}ab}{m\pi\left[(m\pi/k - 1/\tanh(m\pi/k))\sinh m\pi/k - m\pi/k(\cosh(m\pi/k)/\tanh(m\pi/k))\right]} \tag{A.3}$$

and

$$D_{4m} = \frac{-D_{1m}}{\tanh m\pi/k}. \tag{A.4}$$

The stress distribution due to stress function φ_1 is

$$\sigma_{x1} = -\frac{\pi^2}{4b^2}\left(C_1\cosh\left(\frac{k\pi\xi}{2}\right)+C_4\xi\sinh\left(\frac{k\pi\xi}{2}\right)\right)\cos\frac{\pi\eta}{2}, \tag{A.5}$$

$$\sigma_{y1} = \frac{1}{a^2}\left(\left(C_1\frac{k^2\pi^2}{4}+C_4k\pi\right)\cosh\frac{k\pi\xi}{2}+C_4\frac{k^2\pi^2}{4}\xi\sinh\frac{k\pi\xi}{2}\right)\cos\frac{\pi\eta}{2}, \tag{A.6}$$

$$\tau_{xy1} = \frac{\pi}{2ab}\left(\left(C_1\frac{k\pi}{2}+C_4\right)\sinh\frac{k\pi\xi}{2}+C_4\frac{k\pi}{2}\xi\cosh\frac{k\pi\xi}{2}\right)\sin\frac{\pi\eta}{2}. \tag{A.7}$$

The stress distribution due to stress function φ_2 is

$$\sigma_{x2} = \sum_{m=1,2,\ldots}\frac{1}{b^2}\left[\left(D_{1m}\frac{m^2\pi^2}{k^2}+D_{4m}\frac{2m\pi}{k}\right)\cosh\left(\frac{m\pi\eta}{k}\right)+D_{4m}\frac{m^2\pi^2}{k^2}\eta\sinh\left(\frac{m\pi\eta}{k}\right)\right]\cos(m\pi\xi), \tag{A.8}$$

$$\sigma_{y2} = -\sum_{m=1,2,\ldots} \frac{m^2\pi^2}{a^2}\cos(m\pi\xi)\left[D_{1m}\cosh\left(\frac{m\pi\eta}{k}\right) + D_{4m}\eta\sinh\left(\frac{m\pi\eta}{k}\right)\right], \tag{A.9}$$

$$\tau_{xy2} = \sum_{m=1,2,\ldots} \frac{m\pi}{ab}\sin(m\pi\xi)\left[\left(D_{1m}\frac{m\pi}{k} + D_{4m}\right)\sinh\left(\frac{m\pi\eta}{k}\right) + D_{4m}\frac{m\pi}{k}\eta\cosh\left(\frac{m\pi\eta}{k}\right)\right]. \tag{A.10}$$

References

[1] A.W. Leissa, *Vibration of Plates*, US Government Printing Office, NASA SP-160, 1969.

[2] A.W. Leissa, The free vibration of rectangular plates, *Journal of Sound and Vibration* 31 (1973) 257–293.

[3] A.W. Leissa, J.H. Kang, Exact solutions for the free vibrations and buckling of rectangular plates with linearly varying in-plane loading, in: *Proceedings, 2001 ASME International Mechanical Engineering Congress and Exhibition*, New York, 2001, ASME Paper IMECE2001/AD-23758.

[4] J.H. Kang, A.W. Leissa, Vibration and buckling of SS-F-SS-F rectangular plates loaded by in-plane moments, *International Journal of Structural Stability and Dynamics* 1 (2001) 527–543.

[5] S. Timoshenko, J.N. Goodier, *Theory of Elasticity*, 3rd ed., McGraw-Hill Inc., New York, 1970.

[6] G. Pickett, Application of the Fourier method to the solution of certain boundary problems in the theory of elasticity, *Journal of Applied Mechanics* 11 (1944) 176–182.

[7] A. van der Neut, Buckling caused by thermal stresses, High temperature effects in aircraft structures, AGARDograph No.28, 1958, pp. 215–247.

[8] M.B. Benoy, An energy solution for the buckling of rectangular plates under non-uniform in-plane loading, *Aeronautical Journal* 73 (1969) 974–977.

[9] C.W. Bert, K.K. Devarakonda, Buckling of rectangular plates subjected to nonlinearly distributed in-plane loading, *International Journal of Solids and Structures* 40 (16) (2003) 4097–4106.

[10] K.K. Devarakonda, C.W. Bert, Buckling of rectangular plate with nonlinearly distributed compressive loading on two opposite edges, *Mechanics of Advanced Materials and Structures* 11 (4–5) (2004) 433–444.

[11] D.J. Gorman, R.K. Singhal, A superposition-Rayleigh–Ritz method for free vibration analysis of non-uniformly tensioned membranes, *Journal of Sound and Vibration* 162 (3) (1993) 489–501.